New analysis and extensions of split-spectrum processing algorithms

Abstract

In this paper we compare the performances of different variants of split-spectrum algorithms and propose some new extensions based on the use of variable bandwidth filters equally spaced in frequency and energy gain equalized. Signal-to-Noise Ratio Gain and Flaw-to-Clutter Ratio Gain factors were selected as the figures of merit to make the comparisons among the different methods. We considered simulated ultrasonic signals using both stationary and non-stationary models for the grain noise, and real scans obtained in laboratory from low dispersive (aluminum) and high dispersive (cement) materials. Frequency Multiplication (FM) recombination method is revealed as the best option when combined with the new extensions.

Keywords: Split Spectrum, variable bandwidth, frequency multiplication

1 Introduction

One of the main objectives of signal processing techniques in the field of ultrasonic Non Destructive Testing (NDT) is to eliminate or reduce as far as possible the effect of the grain noise to improve the Signal to Noise Ratio (SNR) of echoes in pulse-echo systems [1,2].

Although there are many methods, most of them based on time-frequency decomposition, the most used, due to its simplicity and the good results provided, is the Split Spectrum Processing (SSP) algorithm, widely studied and with a long history in the field of NDT [3]. SSP algorithms exploit the frequency diversity phenomenon [4] that appears in dispersive materials when an ultrasonic wide band pulse is scattered by many small scatterers having sizes comparable to the pulse wavelength. The combined response of all the scatterers is frequency sensitive due to the different phases of every individual contribution. On the contrary, the response of an isolated reflector of enough size will be unique and so frequency insensitive (Fig. 1).

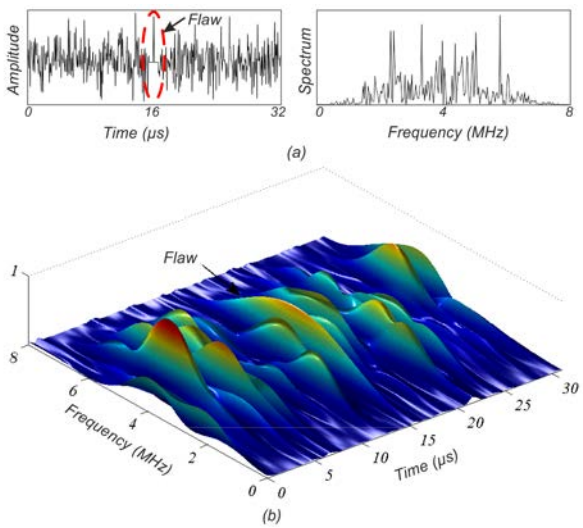

Fig. 1 Example of A-scan with a single defect at 16 μs. (a) Time and Frequency. (b) Normalized Spectrogram. There can be seen the random spectral distribution of the scatterers and how around 16μs the contribution of the defect spreads all around the transmitted bandwidth.

Given an operating bandwidth, the inherent idea in SSP algorithms is to use a filter bank to decompose the received signal followed by a comparison of the different filter outputs, so that, broadly speaking, when all the filter outputs are

similar, the presence of a true defect is enhanced, otherwise, presence of grain noise is reduced (Fig. 2).

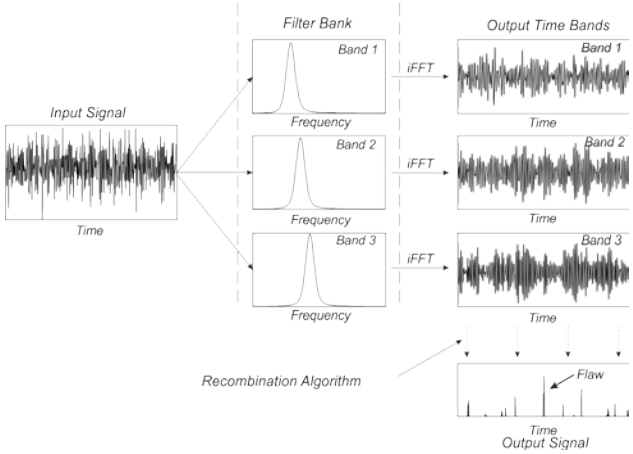

Fig. 2 SSP algorithm schema for a 3 bands filter bank.

Hence, two main parts are given in any SSP algorithm, namely, the filter bank and the recombination technique [2]. In terms of the filter bank, there are two main trends commonly followed. One is based on constant bandwidth filters equally spaced in frequency and the other one uses wavelets as a multi-resolution time-scale method [5][6][7]. In this paper, we introduce a new filter bank prototype based in the combination of both of the previous, using filters of variable bandwidth, as wavelets, but holding its equally distribution pattern along the pulse bandwidth. Other significant difference with wavelets is that we equalize the energy of the bands in order to equalize the amount of energy provided by each band to the analysis.

According to the recombination methods, we will consider in this work five variations. Two of them based on the phase observation, the well known Polarity Thresholding (PT) and the Scaled Polarity Thresholding (SPT), and the other three are some of the classical methods based on Order Statistics (OS)[8], namely Minimization (MIN), Normalized Minimization (NORM) and Geometric Mean (GM). We will use a modification of the last one in which the mean of the product is not calculated, called Frequency Multiplication (FM). This method has not received much attention until now, but will show the best performance in this work, with the advantage that is quiet simple and robust and could be a good choice for its practical real-time hardware and software implementation.

Comparison will be made in terms of Signal-to-Noise-Ratio Gain (SNRG) and Flaw-to-Clutter Ratio Gain (FCRG). We will evaluate the dependence of both parameters on the number of bands, what we will refer across the paper as *efficiency* of the algorithm, and dependence of SNRG on SNR at the input, what we refer across the paper as *sensitivity* of the algorithm.

In the next section we define the new filter bank design introduced in this paper, followed in section 3 by a brief review of the recombination methods used as detectors. Then, section 4 presents the results of comparisons among the proposed structure and the classical filter bank, using the conventional detectors previously described and both simulated and real scans obtained in the laboratory, taking special attention to the modified FM method. Finally, in section 5 we will end with a brief resume and conclusions.

2 New Filter Bank Design

As previously mentioned, we propose an alternative design for the usual filter structure of SSP algorithm using variable bandwidth filters based on the bank of

filters of constant frequency-to-bandwidth ratio (FBR) described in [9], but with some modifications. The structure is basically the same as the classical filter bank, i.e., once fixed the width of the analysis band and the number of bands, the filters are equally distributed across the inspection bandwidth, but now the bandwidth of each filter is selected proportional to its central frequency. Then, bands are energy gain equalized to not affect the frequency distribution of energy at the input signal, as uniformity of that distribution is essential to distinguish the presence of a possible flaw.

In the classical filter bank the filter impulse response of band *i*, using Gaussian filters, can be written as [9,10]:

$$h_i(t) = e^{-\frac{t^2}{2\sigma_i^2}} \tag{1}$$

with F_{ci} the central frequency of the band *i* and σ^2_i the variance of the corresponding Gaussian window, defined as:

$$\sigma_i^2 = \frac{\sqrt{\ln 2}}{2\pi B_i F_{ci}} \tag{2}$$

where B_i is the relative bandwidth at 3dB ($0<B_i<1$) of the filter at band *i*:

$$B_i = \frac{\Delta W \cdot (1 + 2R_{ol})}{L \cdot F_{ci}} \tag{3}$$

which is a function of the operating bandwidth (ΔW), the number of bands (L), the overlap between bands ($0<R_{ol}<1$) and the central frequency of each band F_{ci}). Gaussian filters are commonly used because they provide the best compromise regarding the time-frequency resolution.

In the new design proposed, the relative bandwidth B_i will be the same for all the bands, and considering that bands remain equally distributed, this drives to an implicit energy band equalization and an excess of overlap between bands that will grow with the frequency. Notice that the resulting excess correlation due to this increased band overlapping is not as critical to the performance of the detector as it is selecting the proper frequency range containing significant flaw information [9]. Furthermore, as the bandwidth of the filters is wider than in the classical design, the time resolution improves thus leading to a better location performance.

Other advantage of this architecture is that the overall frequency response of the system is adjusted to that of the transmitted pulse, as we can see if we compare the resulting analyzed bandwidth of the new equalized and equally spaced variable bandwidth filter bank (E-ESVB) of figure 3a with the obtained with the classical filter bank design in figure 3b.

Now, selecting properly the bank parameters (number of filters and bandwidth), all the bandwidth transmitted by the transducer is taken into account for the analysis, fitting it to the frequency response of the material. This configuration will also give greater prominence to the lower frequencies of the band of interest because, as more filters lay on these bands, lower frequencies are analyzed in more detail. According to the Frequency Diversity phenomenon, when the ultrasonic wavefront collides with a reflector comparable to its wavelength, the reflector acts as an omnidirectional and spherical emitter, generating more dispersion at high frequencies than at low frequencies. As a result, it can be said that high dispersive materials act as a low pass filter whose characteristics depend on its composition and the distance that the wave has propagated, attenuating the energy contained mostly in the upper part of the wavefront of the transmitted pulse.

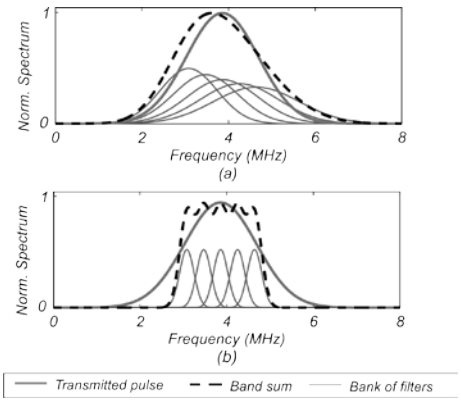

Fig. 3 Normalized Spectrum of the transmitted pulse (continuous line) and the band sum (dotted line) for a 5 bands filter bank. (a) Energy equalized variable bandwidth filters (b) Classical fixed bandwidth filters.

Then, since most of the information remains in the lower frequencies of the inspection band, having more frequency resolution at lower frequencies will be desirable, which we achieve with the E-ESVB. This goal is also achieved with the wavelet analysis, but without the bandwidth adaptation that we get now nor with the time resolution we have with the wider and overlapped filter bank.

The same frequency resolution obtained at low frequencies with the E-ESVB can be also obtained with wavelets or with the constant FBR filter bank. However the time resolution (i.e., resolution in flaw location) worsens substantially. Moreover, these two solutions would require a greater number of bands for the same inspection bandwidth

3 Recombination Methods

Thereafter the following notation will be used; $z_i(n)$ is the SSP output channel i, L is the number of bands and $y(n)=F\{z(n)\}$ is the signal obtained after processing and recombination of the filter bank outputs at n. Thus, algorithms are defined as follows:

- Minimization (MIN)[1,11]:

$$y(n) = \left\{ \min_n |z_i(n)| \right\} \tag{4}$$

- Normalized Minimization (NORM)[12]:

$$\hat{z}_i(n) = \frac{|z_i(n)|}{\max_i z_i(n)} \tag{5}$$

$$y(n) = \left\{ \min_n \{|\hat{z}_i(n)|\} \right\} \tag{6}$$

- Polarity Thresholding (PT)[11,13]:

$$y(n) = \begin{cases} \min_n \{|z_i(n)|\} & \begin{cases} if\ z_i(n) > 0\ \forall n \\ if\ z_i(n) < 0\ \forall n \end{cases} \\ 0 & otherwise \end{cases} \tag{7}$$

- Scaled Polarity Thresholding (SPT)[14]:

$$y(n) = \left| \frac{N_+ - N_-}{N} \right| \cdot \min_n \{|z_i(n)|\} \tag{8}$$

where N_+ and N_- are the number of positive and negative samples respectively and N is the number of samples.

- Frequency Multiplication (FM)[8,11]:

$$y(n) = \prod_{i=0}^{L} |z_i(n)| \tag{9}$$

Note that the geometric mean is not calculated in this case as it is in the classic OS method [15].

4 Results

4.1 Previous Considerations

In order to generalize the study, different stochastic models of grain noise will be used to generate experimental data. We have broadly classified the materials as low or high dispersive. Therefore, we are going to consider two propagation models of the ultrasonic pulse, the first one will be called low-dispersive model (LDM) and the second one high-dispersive model (HDM).

In LDM it is assumed that the ultrasonic pulse remains essentially the same (except for a possible constant attenuation) when it propagates inside the material, thus a linear time invariant system model is possible, where the reflectivity of the material is to be convolved with the sent pulse. From a stochastic perspective, LDM implies a stationary model. The basic equation to simulate LDM is given by [16,17,18]:

$$r(t) = x(t) * \left\{ \sum_{k=1}^{K_s} \rho_{sk} \cdot \delta(t - \tau_{sk}) + \sum_{k=1}^{K_d} \rho_{dk} \cdot \delta(t - \tau_{dk}) \right\} \tag{10}$$

with K_s and K_d the number of scatterers and defects respectively, ρ_{sk} and ρ_{dk} the scatterers and defects reflection coefficients respectively, $\tau_{sk}=2z_{sk}/c_l$ and $\tau_{dk}=2z_{dk}/c_l$ the scatterers and defects locations, c_l the propagation velocity of the ultrasonic wavefront in the material and $x(t)$ the transducer impulse response. In flaw detection approach, the scatterers reflection coefficients are modeled as a white random process, assuming constant the gap between them [19].

In HDM it is assumed that the absorption, scattering and reflection effects of the material microstructure are frequency dependent, hence the pulse suffer significant deformations as it propagates inside the material. Thus a non-linear variant system model is required and non-stationarity appears. The basic equation to simulate HDM is given, in the frequency domain, by [18,20,21]:

$$R(\omega) = X(\omega) \cdot \left\{ \sum_{k=1}^{K_s} \beta \frac{\omega^2}{z_k} \cdot e^{-\alpha_R 2 z_{sk} \omega^2} \cdot e^{-2j\omega z_k / c_l} + \sum_{k=1}^{K_s} \rho_{dk} \cdot e^{-\alpha_R 2 z_{dk} \omega^2} \cdot e^{-2j\omega z_k / c_l} \right\} \tag{11}$$

where $\beta = QV/c^2_l$ is a characteristic constant of the material which depends on the characteristic geometry of the reflectors Q, the analyzed volume V and c_l the propagation velocity of the ultrasonic wavefront in the material [22], a_R is the fraction of the dispersion coefficient in the Rayleigh zone and can be also considered characteristic of the material, z_{sk} and z_{dk} are the scatterers and defects locations, ρ_{dk} are the reflection coefficients of the defects and $X(\omega)$ the transducer impulse response in the frequency domain.

Regarding the transducer, models will be based both on deterministic Gaussian envelope or decreasing exponentials signals, depending on the transducer to be considered. In the first case, the response of the transducer can be modeled using a band-pass signal with Gaussian envelope [10], and in the second one by using a growing potential term combined with a decreasing exponential term, modulated to the desired central frequency [23]. In both cases, the desired waveforms can be achieved by modifying the appropriate parameters. Finally, beamforming techniques [10] can be used to have better control over the transducer frequency response.

We will compare the simulation results with real scans results obtained in the laboratory. For this purpose, we will use a 2MHz transducer with Gaussian envelope (MSW-QGC General Electric) to collect scans from aluminum and a 5MHz transducer with exponential envelope (KBA-5MHz General Electric) to collect scans from cement, both of them focused, so beamforming techniques where included in the models.

To validate the results obtained for low dispersive models, we have chosen an aluminum specimen analyzed with the 2 MHz transducer. At these frequencies, the aluminum alloy used behaves as low dispersive material. The specimen has a 1 cm hole in one of its faces acting as a defect. To simulate this environment, the transducer model used was the Gaussian envelope model centered at 2 MHz and with a 50% bandwidth. Scans were generated with a single delta at defect location with variable reflection coefficient, all immersed in a dispersive environment modeled by the stationary model. Figure 4 shows an example of a simulated scan compared with a real scan.

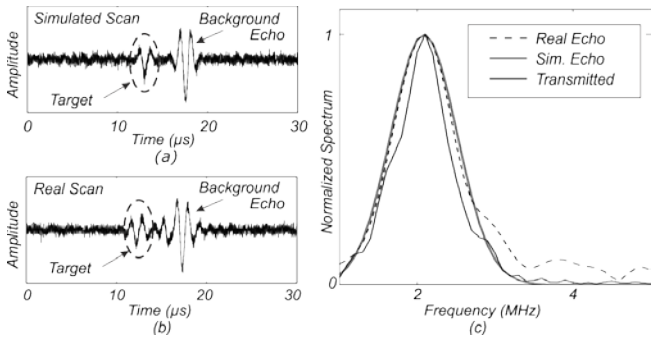

Fig. 4 Comparison in time and frequency of a real aluminum scan and an experimental scan from the stationary model for low dispersive materials (a) Simulated scan (b) Real scan of aluminum with a single defect (c) Corresponding spectra.

For high dispersive materials, we have used cement specimens to validate the results obtained with simulations. In this case the 5 MHz transducer was chosen and the specimen was a block of cement with a defect in the middle of the material with unknown dimensions. At these frequencies, the selected cement specimens (cement 32.5 30% humidity) are very dispersive. To simulate this environment, the transducer model used was a growing potential term combined with a decreasing exponential centered at 5 MHz and with a 50% bandwidth. Scans were generated with a single defect with variable reflection coefficient, all immersed in a dispersive environment modeled by the non-stationary model with attenuation parameter $a_R = 4.86 \cdot 10^{-30}$ and constant $\beta = 5 \cdot 10\text{-}12$ and with 5000 scatterers. Figure 5 shows an example of simulated scan compared with a real scan.

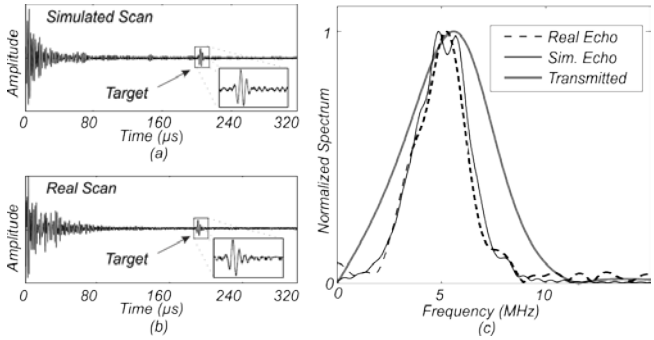

Fig. 5 Comparison in time and frequency of a real cement 32.5 scan and an experimental scan from the non-stationary model for high dispersive materials (a) Simulated scan (b) Real scan of cement with a single defect (c) Corresponding spectra.

In both cases data were collected with *Dasel Ultrascope Usb* hardware and software acquisition system at a sampling frequency of 80 MHz.

In the simulations scenario, the sampling frequency was fixed at 25 MHz, high enough to ensure no lost of resolution compared with the transducer frequencies. In the noise models, certain amount of white noise was added to the scans to take into account the incoherent noise present in the real experiments. In all cases simulations were undertaken according to the Monte Carlo method with 1000 iterations by simulation, varying the number of filters from 2 to 40 bands, repeating the experiment for the two different filter bank designs.

SNRG [4,24] was selected as the figure of merit to make the comparisons among the different methods, measured as the quotient between the Normalized SNR at the input ($NSNR_{IN}$) and Normalized SNR after applying the algorithm *(*$NSNR_{OUT}$):

$$SNRG = \frac{NSNR_{OUT}}{NSNR_{IN}} \tag{12}$$

where

$$NSNR_{OUT} = \frac{\sum_{D+\frac{P}{2}}^{D-\frac{P}{2}} y^2(n)}{\sum_{0}^{N-1} y^2(n)} \tag{13}$$

where *D* is the defect location, P the pulse width and N the record length, all in number of samples. An equivalent definition holds for $NSNR_{IN}$.

Notice that the Normalized SNR has a maximum value of 1 (no noise present) independently of the record length N, thus allowing a better comparison of cases having different records lengths.

The other parameter used for performance evaluation was the Flaw-to-Clutter Ratio Gain (FCRG) [15], measured in dB as the difference between the FCR at the input (FCR_{IN}) and the FCR at the output (FCR_{OUT}) of the algorithm:

$$FCRG = FCR_{OUT} - FCR_{IN} \tag{14}$$

The FCR_{OUT} is calculated as the ratio between the maximum amplitude at the defect location and the largest amplitude of clutter echoes, both after processing the signal:

$$FCR_{OUT} = 20 \cdot \log \frac{F_{OUT}}{C_{OUT}} \tag{15}$$

where F_{OUT} and C_{OUT} are the maximum output echo amplitude of flaw and clutter respectively. An equivalent definition holds for FCR_{IN}.

FCGR gives an indication of the discrimination capability of the algorithm, i.e. how much the algorithm is able to increase the range between the maximum amplitude due to a flaw and the maximum amplitude due to the grain noise.

4.2 Stationary Model. Low Dispersive Materials

Figure 6 shows results obtained for the stationary model after applying the algorithm using both the fixed (left) and variable (right) bandwidth filter banks from 2 to 40 bands in steps of one band and for values of $NSNR_{IN}$ from 0.01 to 0.2 in steps of 0.01.

Figures 6a and 6b show the mean SNRG obtained averaging the gain for each value of $NSNR_{IN}$ considering all the filter banks. Figures 6c and 6d the mean SNRG as a function of the number of bands in the filter bank, averaging for all the $NSNR_{IN}$, and figures 6e and 6f the mean FCRG as a function of the number of bands in the filter bank, averaging for all the $NSNR_{IN}$.

It can be clearly seen that the FM method provides the best values of sensitivity, because it shows the fastest gain increase due to small increasing in the $NSNR_{IN}$ (Fig. 6a), especially when using the new filter bank design (Fig. 6b). Other advantage of this method is that it achieves the highest values of SNRG with the lowest number of bands (Fig 6c and 6d). For the fixed bandwidth filters (Fig. 6a and 6c), PT and SPT reach also high values of gain but they need at least twice the number of bands than FM, and after that PT starts to decay while SPT remains stable in constant values of gain, plus having better sensitivity than PT (Fig. 6a). When using the variable bandwidth filters (Fig. 6b and 6d), neither PT nor SPT are able to denoise the signal.

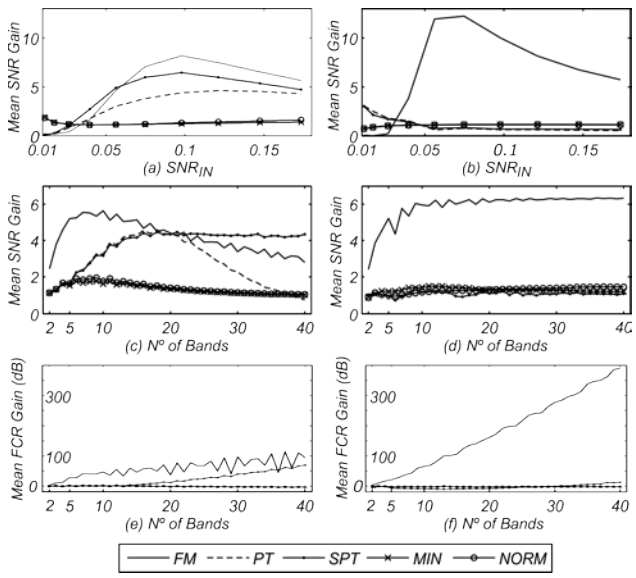

Fig. 6 Stationary-Low Dispersive model. (a)-(b) Mean SNRG vs. $NSNR_{IN}$. (c)-(d) Mean SNRG vs. Nº of Bands. (e)-(f) Mean FCRG vs. Nº of Bands. In all cases left side figures are for fixed bandwidth filters and right side ones for variable bandwidth filters.

If we put our attention in the FCR gain (Figs. 6e and 6f), we see again how the FM method shows the best behavior for both filter bank designs. This is particularly true for the new one, which can achieve values close to 75 dB with only 10 bands.

Finally, regarding the methods based on Minimization, it can be seen that they are neither sensitive nor efficient.

In figures 7a and 7b we show the output obtained after applying the algorithm to a scan using 10 bands. This figure shows again the superiority of the FM method in low dispersive or stationary models. Notice that, even in the case of having reasonable SNRG (PT and SPT) for the selected number of bands, the time records exhibit many false detection, thus indicating that SNRG should be carefully considered when measuring the performance of the different algorithms.

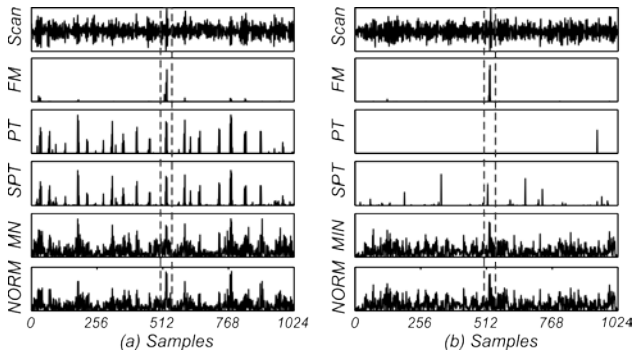

Fig. 7 Stationary-Low Dispersive model. Outputs after recombination for 10 bands and $NSNR_{IN}$=0.1 for (a) fixed and (b) variable bandwidth filters. Selected scan has a single defect at sample 512.

Figure 8 shows results for real scans obtained in the laboratory from the pieces of the aluminum alloy previously described, representative of the low dispersive stationary model that has been used for the experiments. Notice that only efficiency (dependence on the number of bands) is shown, as generating different $NSNR_{IN}$ in a controlled manner was not possible. In any case, results are consistent with those of the foregoing simulations.

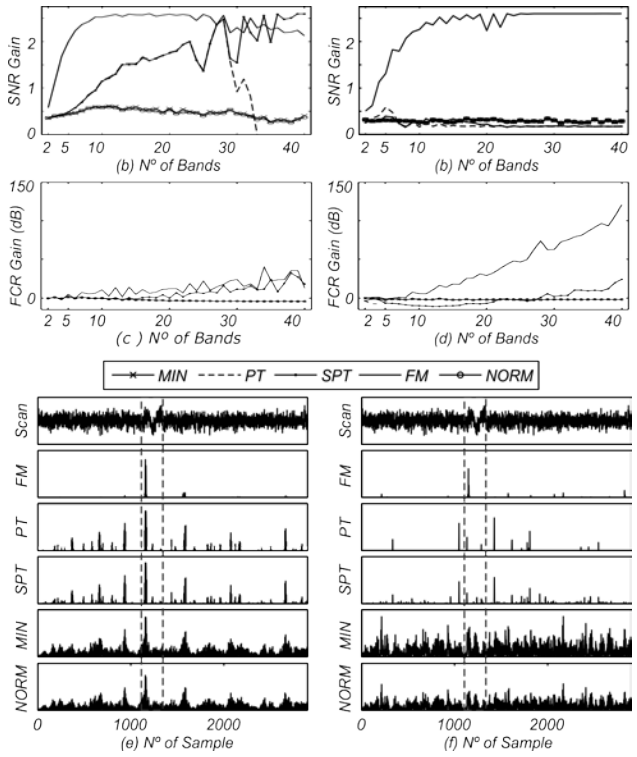

Fig. 8 Results obtained after processing a scan of aluminum with a single defect at sample 1150. SNRG vs. Nº of Bands for (a) fixed and (b) variable bandwidth filters. FCRG vs. Nº of Bands for (c) fixed and (d) variable bandwidth filter. Outputs after recombination of 10 bands for (e) fixed and (f) variable bandwidth filters.

4.3 Non-Stationary Model. High Dispersive Materials

In this case, experiments will be repeated using the non-stationary model assumed to be the most appropriate to simulate the behavior of dispersive materials.

Figures 9a-9b show the mean SNRG obtained averaging the gain for each value of $NSNR_{IN}$ considering all the filter banks, figures 9c-9d and 9e-9f the mean SNRG and mean FCRG respectively as a function of the number of filters in the filter bank, averaging for all the $NSNR_{IN}$. In all cases, left side graphics correspond to classical filter bank and right side ones to the E-ESVB design. Results are shown from 2 to 20 bands only, because over this value no significant changes in the trends were found.

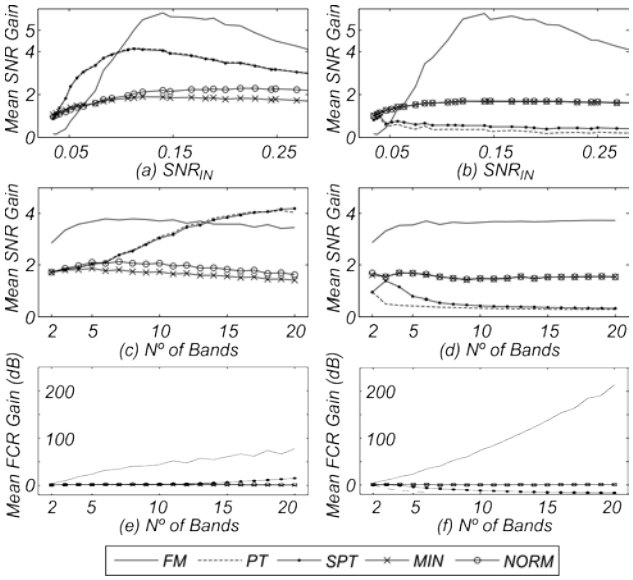

Fig. 9 Non Stationary - High Dispersive model. (a)-(b) Mean SNRG vs. $NSNR_{IN}$. (c)-(d) Mean SNRG vs. Nº of Bands. (e)-(f) Mean FCRG vs. Nº of Bands. In all cases left side figures are for fixed bandwidth filters and right side ones for variable bandwidth filters.

As can be seen (Fig. 9a-9c-9e), with the fixed bandwidth filter bank, FM is again the most sensitive method. It reaches the highest values of SNRG, whereas SPT and PT methods require at least 10 bands to achieve similar values. Moreover, MIN and NORM are again the worst from the point of view of sensitivity and efficiency. In addition, with the new filter bank design, FM improves its sensitivity (Fig. 9b) and gets the maximum gain with a very few bands (Fig. 9d), achieving an extraordinary FCRG even for very low number of bands.

In figures 10a and 10b we show the output obtained after applying the algorithm to a scan using 10 bands. As in the low dispersive case, FM shows the best location performance. Again, although having reasonable SNRG, PT and SPT still exhibit much false detection. MIN and NORM hold their poor resolution, although some improvements are shown when using the new filter bank design.

In general terms, results show again the superiority of FM, especially when the E-ESVB filter bank is used.

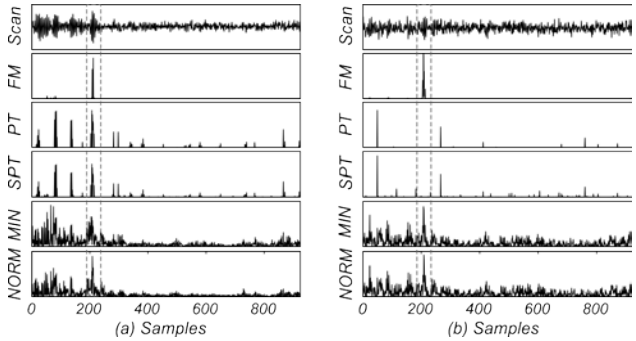

Fig. 10 Non Stationary - High Dispersive model. Outputs after recombination for 10 bands and $NSNR_{IN}$=0.15 for (a) fixed and (b) variable bandwidth filters. Selected scan has a single defect at sample 200.

The last series of figures (Fig. 11) show results for real scans obtained from the cement specimens previously described, representative of the high dispersive non-stationary model. Notice that only efficiency (dependence on the number of bands) and FCRG are shown, as generating different $NSNR_{IN}$ in a controlled manner was not possible. In any case, results are consistent with those of the foregoing simulations.

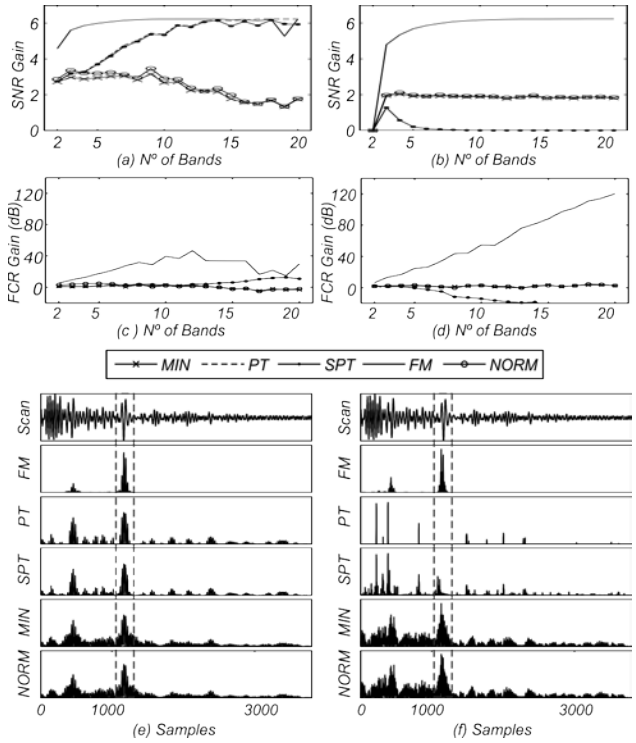

Fig. 11 Results obtained after processing a scan of cement 32.5 with a single defect at sample 1050. SNRG vs. Nº of Bands for (a) fixed and (b) variable bandwidth filters. FCRG vs. Nº of Bands for (c) fixed and (d) variable bandwidth filters. Outputs after recombination of 10 bands for (e) fixed and (f) variable bandwidth filters.

5 Conclusion

We have presented an experimental comparison among some representative variations of the SSP algorithms. Five variations were selected: MIN, NORM, PT, SPT and FM. NORM and SPT are respective extensions of MIN and PT, although SPT may be also considered an hybrid method between MIN and PT. FM is a variation of the Geometric Mean OS method. Experiments have been exhaustive to obtain conclusions that could be generalized. For this purpose, simulations were performed

with materials of different degrees of dispersion. Additionally, real data experiments were carried with samples of aluminum and cement. Comparisons were made in terms of sensitivity (dependence of the SNRG with the $NSNR_{IN}$) and efficiency (dependence of the SNRG and the FCRG with the number of bands). Moreover, time records for some representative configurations have been showed to obtain more evidences of the actual performance of the methods, in especial in what concerns the number of false echoes detected.

It has been proposed a new design for the filter bank, which uses variable bandwidth filters equally spaced in frequency and energy equalized. That has shown to be the most efficient option from two different perspectives. First, it reaches the highest SNR Gain with the lowest number of bands. Second, it achieves very high values of the FCR, thus making much easier the detection process.

Some significant conclusions have been reached:

- FM has showed to be the best recombination method in most cases, from the point of view of sensitivity, efficiency and lacking of false detections.
- PT and SPT exhibit similar sensitivity and efficiency, always superior to MIN and NORM, but generally worse than FM. However, the output time of PT and SPT show too many false echoes, which can be a practical limitation, especially when automatic detection of echoes is required. In addition of that, the achieved FCR will always be much lower than with the FM method.
- FM improves significantly when using the new filter bank design. However PT and SPT degrade, and MIN and NORM remain basically unaffected.
- The combination of the new filter bank proposed with the FM method is able to provide values close to 60 dB in the FCR_{OUT} with a low number of bands, what makes this combination an interesting option when automatic detection is required.

As a main conclusion we can say that FM in conjunction with the new E-ESVB filter bank has showed to be a very attractive SSP method. This is in contrast with the few attention received in the past by the FM recombination technique.

Acknowledgment

This work has been supported by the Ministerio de Fomento (Spain) and the Ministerio de Ciencia e Innovación (Spain), and FEDER funds under the projects T39/2006, TEC2008-06728 and TEC2008-02975

References

[1] Newhouse VL, Bilgutay NM, Sniie J, Furgason . Flaw-to-grain echo enhancement by split-spectrum processing. Ultrasonics 1982;20(2):59–68.

[2] Bilgutay NM, Sniie J. The effect of grain size on flaw visibility enhancement using split spectrum processing. Mater Eval 1984;42(6):808–14.

[3] Rubbers P, Pritchard CJ. An overview of split spectrum processing. NDTnet 2003;8(8).

[4] Tian Q, Bilgutay NM. Statistical analysis of split spectrum processing for multiple target detection. IEEE Trans Ultrason Ferroelectr Freq Control 1998;45(1):251–6.

[5] Drai R, Khelil M, Benchaala A. Time frequency and wavelet transform applied to selected problems in ultrasonics. NDT&E International 2002;35:567–72.

[6] Legendre S, Goyette J, Massicotte D. Ultrasonic nde of composite material structures using wavelet coefficients. NDT&E International 2001;34:31–7.

[7] Le Gonidec Y, Conil F, Gibert D. The wavelet response as a multiescale ndt method. Ultrasonics 2003;41:487–97.

[8] Saniie J, Nagle DT, Donohue KD. Analysis of order statistic filters applied to ultrasonic flaw detection using split-spectrum processing. IEEE Trans Ultrason Ferroelectr Freq Control 1991;38(52):133–40.

[9] Aussel JD. Split-spectrum processing with finite impulse response filters of constant frequency-to-bandwidth ratio. Ultrasonics 1990;28:229–40.

[10] Cincotti G, Cardone G, Gori P, Pappalardo M. Efficient transmit beamforming in pulse-echo ultrasonic imaging. IEEE Trans Ultrason Ferroelectr Freq Control 1999;46(6):1450–8.

[11] Karaoguz M, Bbilgutay N, Akgul T, Popovics S. Defect detection inconcrete using split spectrum processing. Proc IEEE Ultrason Symp 1998 1998;1:843–6.

[12] Bosch I, Vergara L. Normalized split-spectrum: A detection approach. Ultrasonics 2008;48:56–65.

[13] Shankar PM, Karpur P, Newhouse VL, Rose JL. Split spectrum processing: Analysis of polarity thresholding algorithm for improvement of signal-to-noise ratio and detectability in ultrasonic signals. IEEE Trans Ultrason Ferroelectr Freq Control 1989;36(1):101–8.

[14] Nguyen TQ, Jayasimha S. Polarity-coincidence filter banks and nondestructive evaluation. Proc ISCAS 1994 1994;2:497–500.

[15] Yoon S, Oruklu E, Saniie J. Performance evaluation of neural network based ultrasonic flaw detection. Proc IEEE Ultrason Symp 2007 2008;:1579–82.

[16] Saniie J, Wang T, Bilgutay M. Statistical evaluation of backscattered ultrasonic grain signals. J Acoust Soc Am 1988;84(1):400–8.

[17] Wagner RF, Smith SW, Sandrik JM, Lopez H. Statistics of speckle in ultrasound b-scans. IEEE Trans on Sonics and Ultras 1983;30(3):156–63.

[18] Donohue KD. Maximum likelihood estimation of a-scan amplitudes for coherent targets in media of unresolvable scatterers. IEEE Trans Ultrason Ferroelectr Freq Control 1992;39(3):422–31.

[19] Karpur P, Canelones OJ. Split spectrum processing: a new filtering approach for improved signal to noise ratio enhancement of ultrasonic signals. Ultrasonics 1992;30(6):351–7.

[20] Gustafsson MG. Nonlinear clutter suppression using split spectrum processing and optimal detection. IEEE Trans Ultrason Ferroelectr Freq Control 1996;43(1):109–24.

[21] Gustafsson MG, Stepinski T. Studies of split spectrum processing, optimal detection, and maximum likelihood amplitude stimation using simple clutter model. Ultrasonics 1997;35:31–52.

[22] Kino GS. Acoustic waves: devices, imaging, and analog signal processing. Prentice-Hall Inc.; 1987.

[23] Kuc RB. Application of kalman filtering techniques to diagnostic ultrasound. Ultrason Imaging 1979;1(2):105–20.

[24] Tian Q, Bilgutay NM. Statistical analysis of split spectrum processing. Proc IEEE Ultrason Symp 1996 1996;:709–12.